Acoustical properties of an immersed corner -cube retroreflector alone and behind screen for ultrasonic telemetry applications

Marie-Aude Ploix, Pierre Kauffmann, Jean François Chaix, Ivan Lillamand, François Baqué, Gilles Corneloup

Acoustical properties of an immersed Corner-Cube Retroreflector alone and behind screen for ultrasonic telemetry applications

Marie-Aude Ploix[1]*, Pierre Kauffmann[1], Jean-François Chaix[1], Ivan Lillamand[1], François Baqué[2], Gilles Corneloup[1]

[1]Aix Marseille Univ, CNRS, Centrale Marseille, LMA UMR 7031, Avenue Gaston Berger, 13625 Aix-en-Provence Cedex, France

[2]CEA Cadarache, DEN/DTN/STCP/LISM, 13108 St Paul lez Durance, France

*Corresponding author:

E-mail: marie-aude.ploix@univ-amu.fr

Phone: +33 (0)4 42 93 90 34

Abstract:

Ultrasonic telemetry measurements consist in remotely detecting and locating an object. To maximize the signal-to-noise ratio, a target may be used, positioned at a reference point. In this framework, the ultrasonic reflective characteristics of a corner-cube retroreflector (CCR) are investigated. The most interesting property of a CCR is its ability to fully reverse an incoming wave in the same direction under certain conditions. Theoretical developments are performed in order to understand its acoustic behaviour, and experimentations are made in various configurations: CCR alone in water, and behind an immersed plate that acts as a screen, with normal and non-normal incidence. The results highlight its strong performance. Moreover, the study of two other couples of CCR material and surrounding fluid underlines the relevance of considering the acoustic properties of each medium, as they have a strong influence on the acoustic response of the CCR.

Keywords: Corner-Cube Retroreflector; trihedral reflector; acoustical properties; ultrasonic telemetry; telemetry behind screen(s)

1. Introduction and state of the art

The concept of sodium-cooled fast reactor (SFR) is being studied in France for the 4th generation of nuclear power plants [1]. The improvement of in-service inspection and repair (ISI&R) is a major issue in the case of nuclear power plants. Ultrasonic solutions are particularly adapted to this harsh environment, and are therefore being studied for the inspection of the main vessel and its internal components. In this context, different methods to perform ultrasonic NDT and NDE are being investigated by CEA and its partners [2].

Localisation and positioning of an object by using ultrasounds require an appropriate relative orientation between the object and the ultrasonic beam. In pulse-echo mode, sufficient specular energy has to travel back towards the transducer to be analysed and interpreted. This condition may fail to occur for example in the case of a misaligned or nonplanar object. A solution studied here consists in using of a specific target part attached to the object, this target being designed to reflect well towards the emitter. The Corner-Cube Retroreflector (CCR), also named retroreflector, corner reflector or trihedral rectangular reflector in the literature, is an efficient target found to reflect incoming waves back to the emitter even when these incoming waves do not strike it perpendicularly (over a certain angular range, about ±30°). Retroreflectors are common in everyday life, in the field of optics [3,4] (for example as security reflectors on bikes), or for advanced technological applications, such as satellite and lunar laser ranging systems [5,6], or else with radar waves for geophysical observations and monitoring [7–11].

In the field of ultrasound, CCR targets remain rather unknown despite their obvious efficiency. A few authors [12–18] propose various ultrasonic reflectors (conical, linear, trihedral etc.) for very specific applications, such as transducer characterisation or determination of misalignment of a transducer. For telemetry applications, CCR seems the best candidate because not only does it send back a lot of energy even if misaligned but also it provides an easy-to-detect spatial reference. However, no extensive study was really performed on the acoustical properties of a CCR alone or behind screens.

A CCR acts as a planar reflector (waves are reflected parallel to the incidence direction) even off “normal incidence”, and the reflection can be total under certain conditions. The reflected amplitude level depends on the angular incidence, on the alignment of the transducer with the CCR inner vertex and on the two media (CCR material and surrounding liquid). It is more or less equivalent to a corner effect, but in 3D. The main developments (theoretical and experimental) are performed here in water, but the ultimate objective is telemetry applications in liquid sodium. Thus to try to get closer to this case, a CCR made of copper is also studied. This paper aims at reviewing and enhancing knowledge of the acoustical properties of a CCR, from a theoretical and experimental point of view, in the general framework of ultrasonic telemetry on an object which may have moved out of position and potentially hidden by one (or several) immersed plate(s). In this case the target is fixed on the object of interest.

Section 2 presents the theoretical background and results. Then experimentations in various configurations are detailed and analysed in section 3. Finally, in section 4 we

study the influence of different acoustic properties of the CCR material and the surrounding fluid.

2. Theoretical background and modelling

A CCR consists of three mutually orthogonal planes (isosceles right triangular faces) joining the inner vertex as schematized in Figure 1a. In the following, the "incidence angle" on the CCR designates the incidence relative to the reference plane (X_2X_3) which is the cutting plane of the cube the CCR is virtually obtained from. An incident ray, non-aligned with the vertex, will reflect successively on the three faces (with a different local incidence on each face) and will result in a final reflected ray parallel to the initial incident one. Figure 1b shows examples of incident rays and their successive reflections with respect to Snell's law.

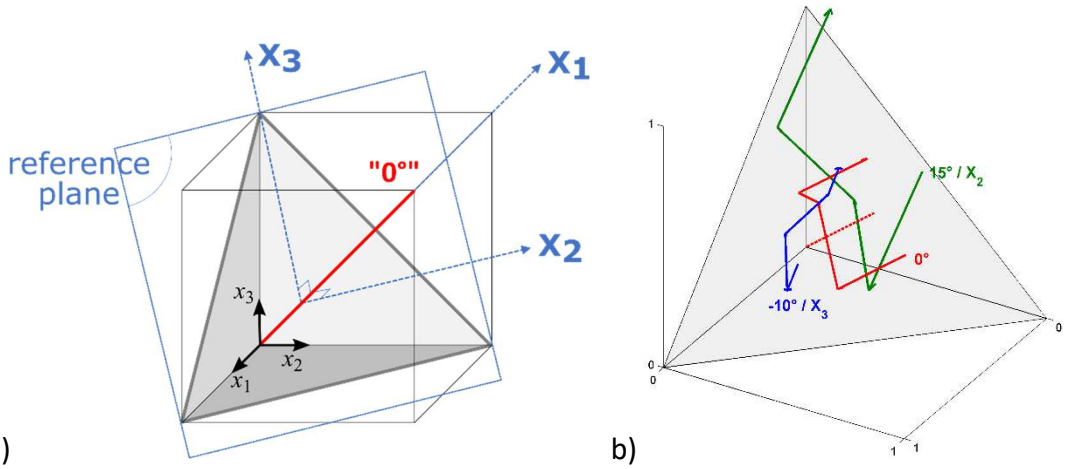

a) b)

Figure 1: a) Definition of coordinate systems, and normal incidence, referred to as "0°" and b) examples of successive reflections of a ray on the faces with various incidences

Moreover, after the three reflections, the times-of-flight of all the rays are the same in the plane parallel to (X_2X_3) containing the ray starting point, equal to the time-of-flight

100 of the travel on the X_1-axis impacting the inner corner of the target. Then the
101 calculation of the distance from the time-of-flight will provide the distance between
102 the transducer and the inner corner of the target.
103 Note that there are ineffective (shadow) areas of the CCR that reflect an incident ray
104 only partially (one or two reflections instead of three). For normal incidence, such
105 areas are the three triangles sizing a third of the CCR side located at the three
106 endpoints of the CCR [7,11].
107
108 If we consider now the contour of the incident beam (modelled by a set of rays
109 cylindrically arranged), it can be easily known whether the reflected beam will merge
110 with the incident beam or not. As shown by the examples in Figure 2, whatever the
111 incidence angle, if the reflected beam exists (in terms of amplitude, see below), it will
112 merge with the incident beam only if the latter is aligned with the inner vertex of the
113 CCR. Otherwise the reflected beam is shifted from the initial incident beam location,
114 the angle of propagation remaining the same.
115

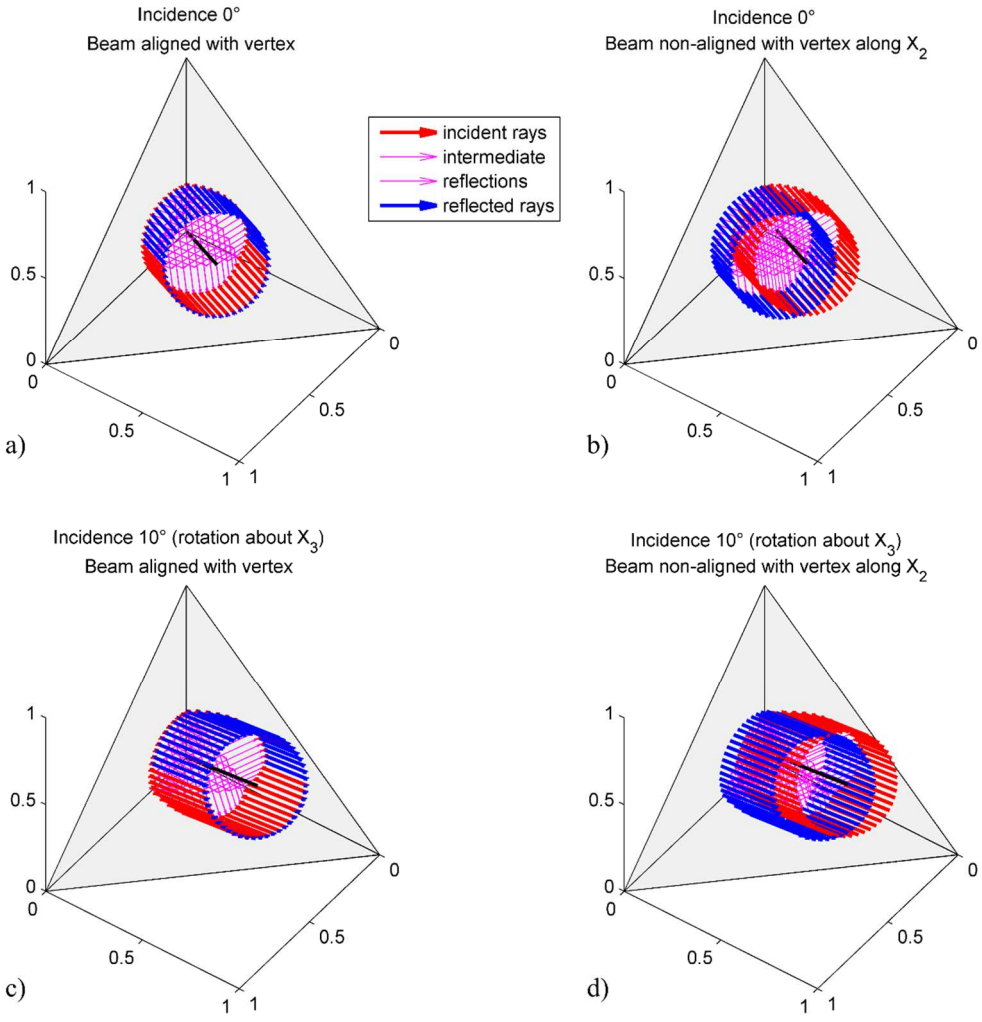

Figure 2: Calculation of cylindrical beam reflection as a function of the angle of incidence and the alignment with the inner vertex (the total length of the arrows of one ray travel corresponds to a single time-of-flight)

The overall reflected amplitude depends on the successive local reflections on the CCR faces. If we consider an incident direction noted $\overrightarrow{U_{inc}}$ (normalized vector) in the coordinate system ($X_1X_2X_3$), it becomes $\overrightarrow{u_{inc}}$ in the coordinate system ($x_1x_2x_3$):

$$\overrightarrow{u_{inc}} = M\overrightarrow{U_{inc}}$$

where $M = \begin{bmatrix} \sqrt{3}/3 & -\sqrt{2}/2 & -\sqrt{6}/6 \\ \sqrt{3}/3 & \sqrt{2}/2 & -\sqrt{6}/6 \\ \sqrt{3}/3 & 0 & \sqrt{6}/3 \end{bmatrix}$ is the transformation matrix between the two coordinate systems.

The local incidence angles on each face are thus given by:

$$\alpha_{(x_1x_2)} = cos^{-1}\left(-\overrightarrow{u_{inc}}.\begin{bmatrix}0\\0\\1\end{bmatrix}\right)$$

$$\alpha_{(x_1x_3)} = cos^{-1}\left(-\overrightarrow{u_{inc}}.\begin{bmatrix}0\\1\\0\end{bmatrix}\right)$$

$$\alpha_{(x_2x_3)} = cos^{-1}\left(-\overrightarrow{u_{inc}}.\begin{bmatrix}1\\0\\0\end{bmatrix}\right)$$

At normal incidence for example (i.e. $\overrightarrow{U_{inc}} = -\overrightarrow{X_1}$), the three local incidence angles are equal, and their value is about 54.7°. The theoretical reflection coefficient [19,20] in the case of water as surrounding liquid and stainless steel as CCR metal is displayed in Figure 3. The two critical angles are 14.9° for the disappearance of longitudinal waves and 28.2° for the disappearance of transversal waves, and conversion into Rayleigh wave occurs at 30.7°. It can therefore be concluded that local reflection on one face is total at 54.7° incidence and thus global reflection at “normal incidence” on the CCR is total. Therefore, in water, at normal incidence, a steel CCR is more efficient as a reflector than a steel plate, provided that the CCR is larger than the beam.

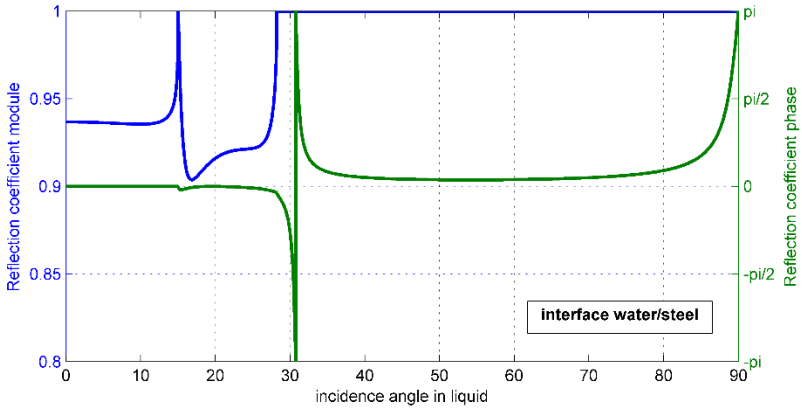

Figure 3: Reflection coefficient (module and phase) at the water/steel interface as a function of the incidence angle

Moreover if we consider arbitrary incidence on a geometrically infinite CCR, the calculation of local incidence angles on each face (see Figure 4) coupled with the reflection coefficient of Figure 3 makes it possible to conclude that:

- For incidence angles about the X_3-axis from -36° to +36° (incidence in X_1X_2 plane), the global reflection is always total, except in the cases of Rayleigh wave generation at -31.1° and +31.1°. For incidence angles between 36° and 40°, some energy is transferred into the metal thanks to its conversion into transversal waves. The global reflection will thus be weaker.
- For incidence angles about the X_2-axis from -40° to +26.7° (incidence in X_1X_3 plane), the global reflection is always total, except in the cases of Rayleigh wave generation at +24°. Beyond 26.8° a part of the incident energy is converted into transversal waves in the steel.

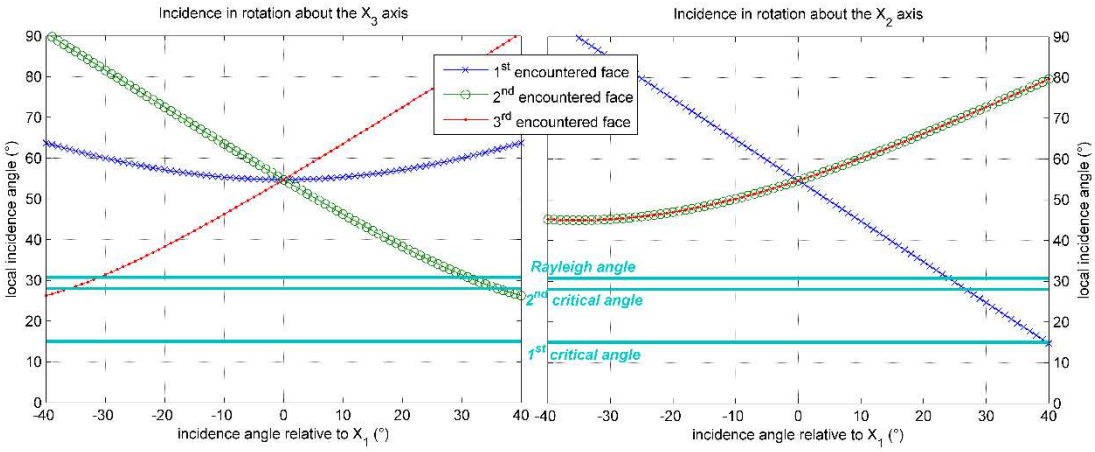

159

160 Figure 4: Local incidence angles on the faces as a function of the initial incidence on CCR

161

162 Three physical phenomena can reduce the amplitude of an arbitrary incident beam
163 reflected from a CCR: 1) energy is converted into Rayleigh waves on one face, 2) the
164 bulk reflection on one face is not total, which happens rather rarely in the case of steel
165 in water, or 3) due to the finite dimensions of the CCR regardless of the beam
166 diameter, a part of the energy is lost (the beam reaches ineffective areas and is
167 reflected only once or twice, or a part of the incident beam strikes off the target area,
168 or the reflected beam is shifted and therefore not entirely incident onto the
169 transducer).

170

171 These phenomena are taken into account in our model using the CIVA expertise
172 platform [21]. The CCR is imported from CAD software. A rotational scan in echo mode,
173 centred on the inner CCR vertex, is computed (Figure 5.a), and the maximum reflected
174 amplitude is plotted as a function of the incidence angle (Figure 5.b). The maximum
175 reflected amplitude occurs at 0°, and it decreases slowly to reach a minimum at 36°.

In our case of computation of echoes from an immersed target, the CIVA model is invalid in the near vicinity of the longitudinal, transversal and Rayleigh critical angles. Indeed this model based on the Kirchhoff approximation [22,23] does not take into account head waves or Rayleigh waves and uses the plane wave reflection coefficient which is discontinuous in terms of magnitude or phase at these critical angles. Nevertheless, to simulate the response of flaws inside a solid specimen, CIVA mimics some head waves using its semi-analytical PTD (Physical Theory of Diffraction) model [24,25] and head/Rayleigh waves are henceforth correctly modelled in the CIVA hybrid ECHO model [26] using the Finite Elements method for flaw modelling.

The CIVA result presented below will be confronted with experimentation in the next section.

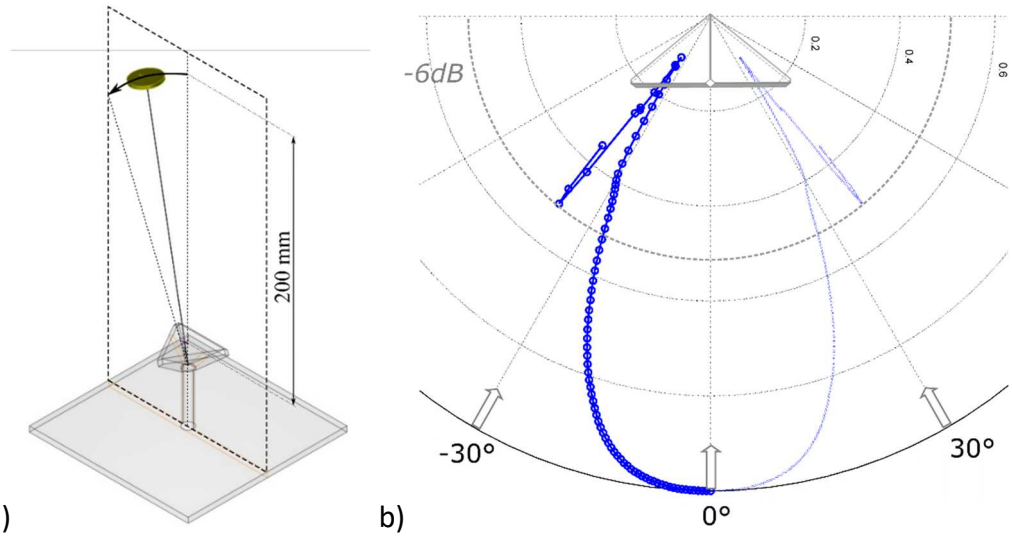

a) b)

Figure 5: Rotational scan about X_3 on CIVA: (a) configuration and (b) polar plot of the maximum received amplitude

3. Experimentations for various configurations

Experimental measurements are performed in immersion, in water at room temperature as a first step. The 43mm side stainless steel CCR is fixed on a plate (see Figure 6). The ultrasonic emitter-receiver is a flat transducer, 1”-diameter, broadband, centred at 2.25MHz. It is first set so as to be aligned with the inner vertex of the CCR at 0° incidence, at about 200mm from the cutting plane (X_2X_3) of the CCR.

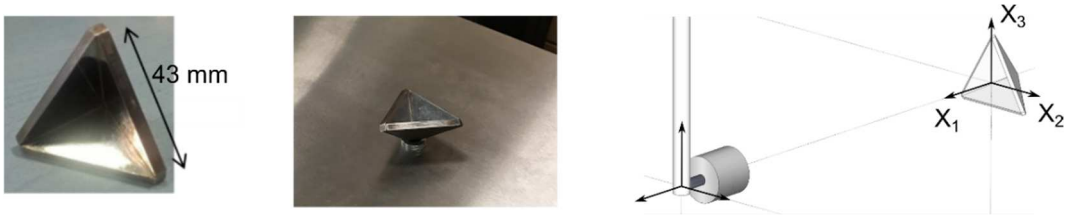

Figure 6: Stainless steel CCR and experimental setup

3.1. Validation of modelling

Bscan type acquisitions (1D scanning) are made along the X_2 axis for various incidence angles of the beam, from 0° to 40° by steps of 1°. For each angle, the position at which the incident beam is aligned with the vertex of the CCR corresponds to the maximum reflected amplitude because there is no beam shift in this position (see Figure 2).

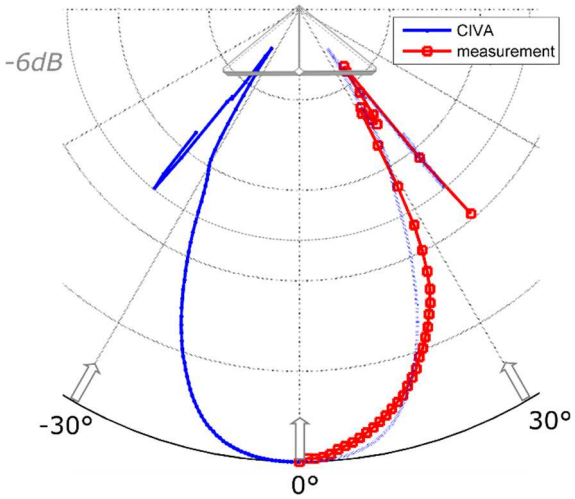

Figure 7: Polar plot of the maximum reflected amplitude: comparison between CIVA simulations and experimentation

The maximum reflected amplitude value is then saved and plotted as a function of the incidence angle in Figure 7 along with CIVA results. The agreement between simulation and experimentation is quite good (except at the Rayleigh angle, as previously explained). This will allow the use of CIVA in more complex cases as will be seen in section 4.

3.2. Ultrasonic field reflected by a CCR alone

Cscan type acquisitions (2D scanning) are performed over the area of the target, parallel to (X_2X_3), in order to analyse how it reflects the beam. Results at 0° incidence (amplitude and time-of-flight) are displayed in Figure 8 for different choices of time-domain windowing: a global window over all the received echoes (including those reflected on the plate carrying the CCR), a window focusing around the time-of-flight from the inner vertex of the CCR, and a window centred on the weak echoes coming back from its edges.

Global reflections from the CCR and the supporting plate are plotted in Figure 8.a. The amplitude image (left) shows up the position of the CCR on the plate and confirms that the maximal amplitude from the CCR is registered when the acoustic beam is aligned with the CCR inner vertex. As expected, the corresponding time-of-flight (right) is constant and is equivalent to the direct path to the CCR inner vertex. The tightened windowing on the CCR inner vertex echoes only (Figure 8.b) highlights the field sent back by the CCR and the constant time-of-flight. This treatment makes it possible to

check the proper angular positioning of the target against the transducer. As for the last windowing (Figure 8.c) around echoes from the edges, its plot also confirms that the CCR is well positioned. However, the amplitudes are weak because the echoes are generated by scattering (or diffraction).

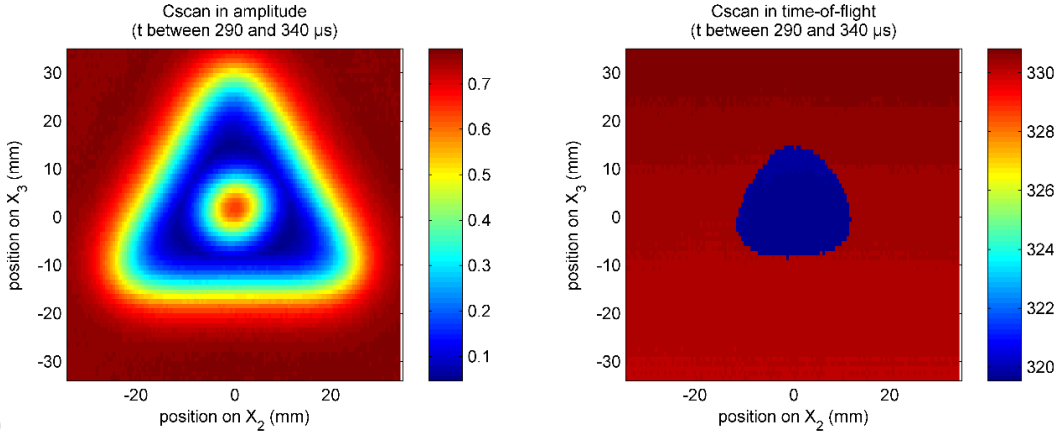

a)

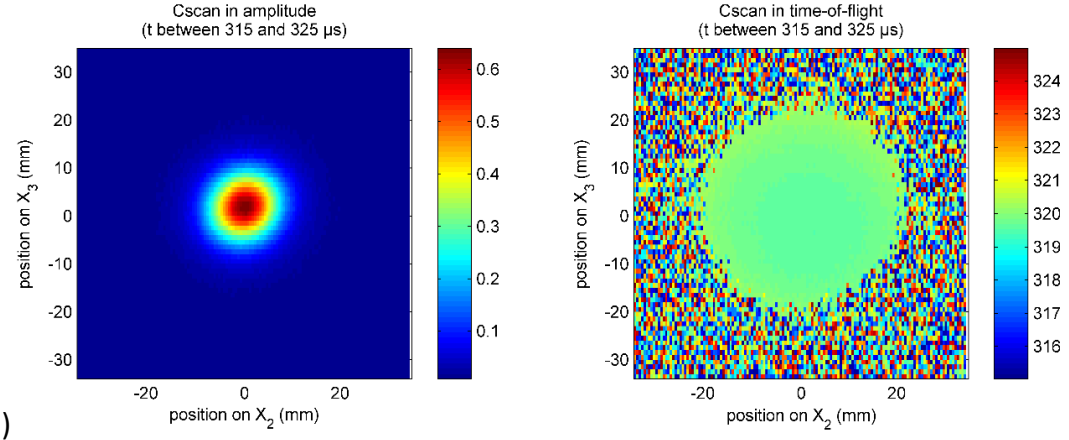

b)

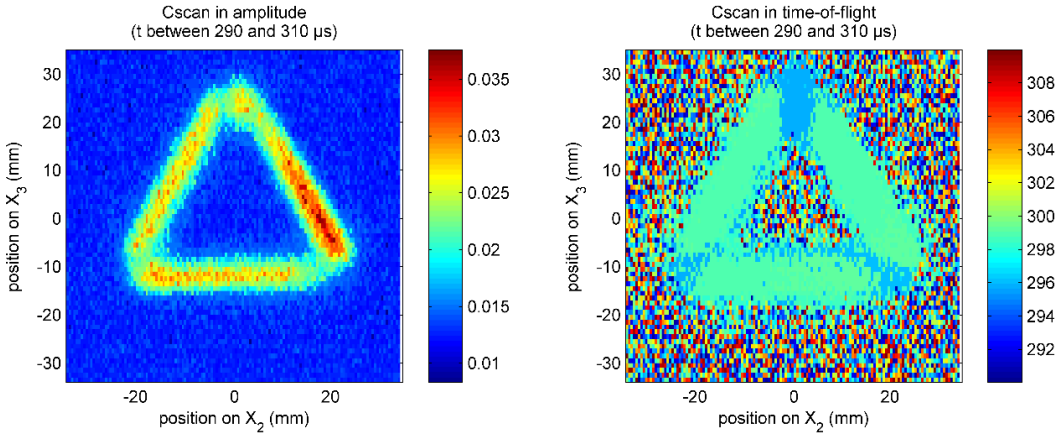

c)

Figure 8: Normal incidence Cscan images in amplitude (left) and time-of-flight (right): a) global windowing, b) windowing on CCR inner corner echoes, and c) on CCR edges

These acquisitions are made for various incidence angles (transducer tilted around X_3, and scanned plane always parallel to (X_2X_3)). At oblique incidence, the time-of-flight is not constant anymore but evolves linearly as a function of the inclination of the transducer with respect to the scanned plane. The edges are not visible anymore. An example of such acquisition is shown in Figure 9. The maximum of amplitude is again reached when the acoustic beam is aligned with the CCR vertex.

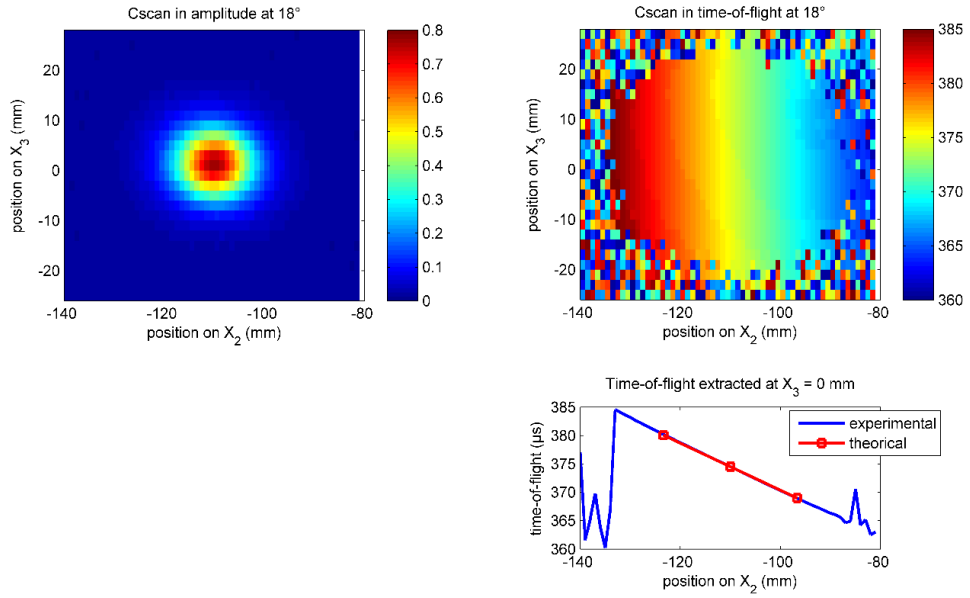

Figure 9: Example of Cscan acquisition at oblique incidence (18°): in amplitude (left) and in time-of-flight(right)

3.3. Ultrasonic response of a CCR behind a plate

The purpose of this study is to perform telemetry on an object equipped with a CCR and located behind a plate. This 7.8 mm thick 316L stainless steel plate is positioned parallel to the scanning plane (X_2X_3).

At normal incidence, each time the beam passes through the plate, it loses about 90% of its energy in reflection. However, the CCR is still well identified, as shown in Figure 10, provided that its echoes do not overlap other echoes, such as those resulting from the multiple round trips between the transducer and the plate hiding the target.

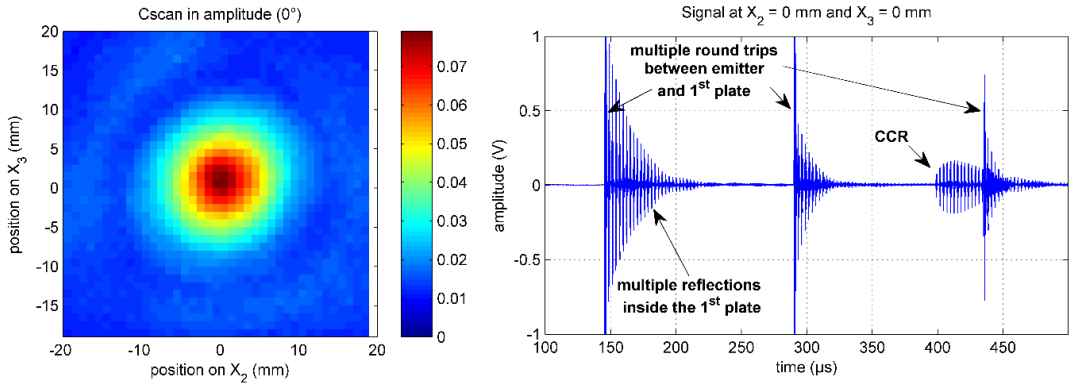

Figure 10: Acquisition at normal incidence on the CCR behind a plate (Cscan with narrow time window focused on the first echo from the CCR, between 398.5 and 400 µs)

Thus, positioning the transducer at oblique incidence will eliminate the problem of multiple echoes. Moreover, the energy transmitted through the first plate can be increased if the incidence angle is well chosen. Therefore, the transmission coefficients through a steel plate immersed in water are calculated and plotted in Figure 11. The maximum of transmission is reached for an incidence around 17°, generating shear waves at about 40° in the plate. We fix here the incidence angle at 18°, because it

corresponds to the maximum of transmission measured experimentally using our setup.

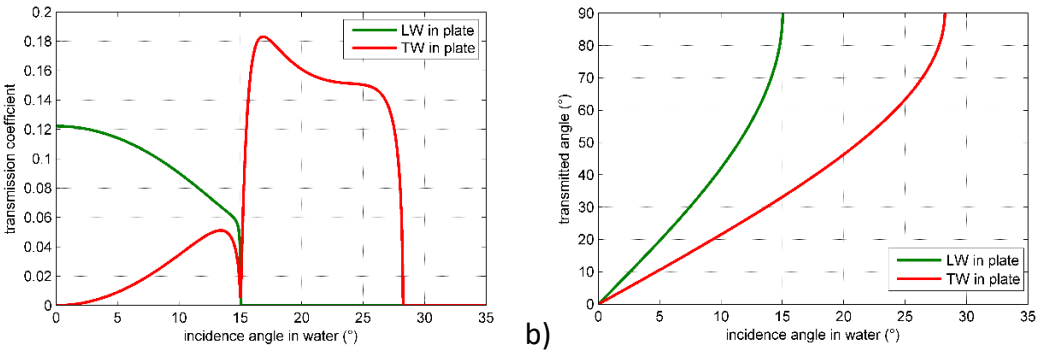

a) b)

Figure 11: a) Transmission coefficient (separate contribution of longitudinal and transverse waves) through a steel plate immersed in water. b) Angle of propagation in the plate, as a function of the incidence angle

Resulting Cscan images (amplitude and time-of-flight) are plotted in the upper part of the Figure 12a. Again, the CCR is clearly identifiable and its ultrasonic image is visible with the repetition corresponding to the successive oblique reflections in the plate. As previously the time-of-flight evolves linearly with the displacement of the transducer, and exhibits steps corresponding to the increase in the number of round trips in the plate.

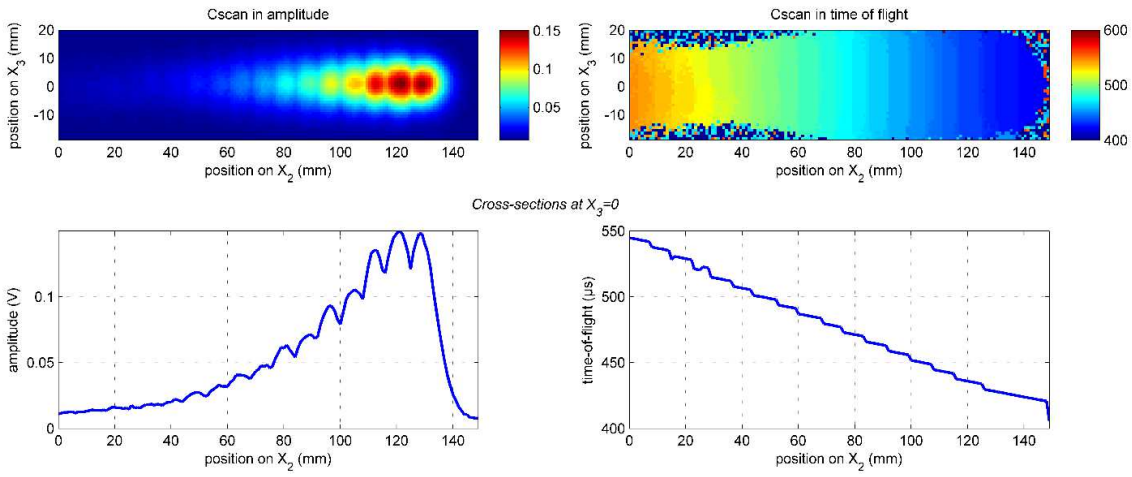

a)

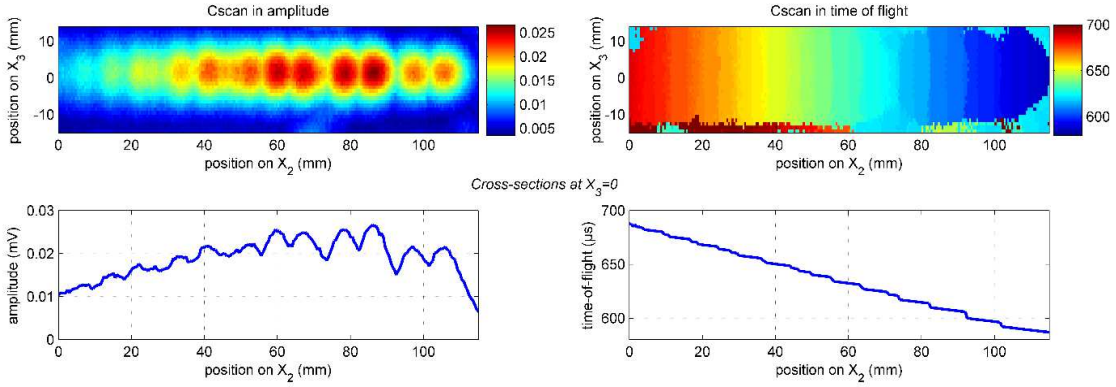

b)

Figure 12: Acquisition at oblique incidence (18°) on the CCR (a) behind one plate, and (b) behind two plates

Signal-to-noise ratios (SNR) were estimated on the acquired maximal signal in each case (at normal and oblique incidence, alone and behind one and two screens), and orders of magnitude are indicated in Table 1. The similar experiments conducted with two screens (parallel plates) behind the target show that the target is not visible at normal incidence but clearly identifiable at oblique incidence (see Figure 12b). All these results clearly highlight how improved the back echo amplitude is when a CCR is adding on the object of interest for detection purposes and telemetry applications.

Configuration	CCR alone (normal incidence)	CCR behind a plate, normal incidence	CCR behind a plate, oblique incidence (18°)	CCR behind two plates, normal incidence	CCR behind two plates, oblique incidence (18°)
SNR / inner corner	more than 100	about 8 (when non-	about 50	/	about 3

		overlapping)			
SNR / edges	about 2	/	/	/	/

Table 1: Signal-to-noise ratio estimated of the back echoes from the CCR according to configuration

4. Discussion on the change of materials: stainless steel in liquid sodium and copper in water

The case of a stainless steel CCR immersed in water is well adapted for detection and telemetry operations in 2nd and 3rd generation nuclear power plants, but not for the 4th generation reactors, in which liquid sodium is used as coolant [27]. Ultrasound propagates faster in liquid sodium than in water (2470 $m.s^{-1}$ in sodium at 200°C [28]), and this shifts all the critical angles up: the first and second critical angles are now 25.5° and 51.7°, and the Rayleigh angle is now 58°, instead of 14.9°, 28.2° and 31.5°. This means that the angular range with total reflection on the CCR is null because no incidence angle allows total reflection locally on all the three faces (cf. Figure 13.a). This leads to a modelled reflection diagram (Figure 14.a) very different from the one for the previous case. The global reflection is no longer maximal at normal incidence, and in particular there are two local minima, at 0° and 10°.

Validation tests are not easy to perform in liquid sodium, as its handling requires special safety precautions. That is why we searched for another (common) material whose behaviour in water would be similar to that of steel in liquid sodium. Then we calculated critical angles and reflection coefficients for various materials and chose copper. In fact, the critical angles for copper in water are close to what they are for

steel in liquid sodium (18.5°, 40.4° and 43.9°), as shown in Figure 13.b. A narrow range of incidence angle leading to total reflection remains, from about -8° to 8°.

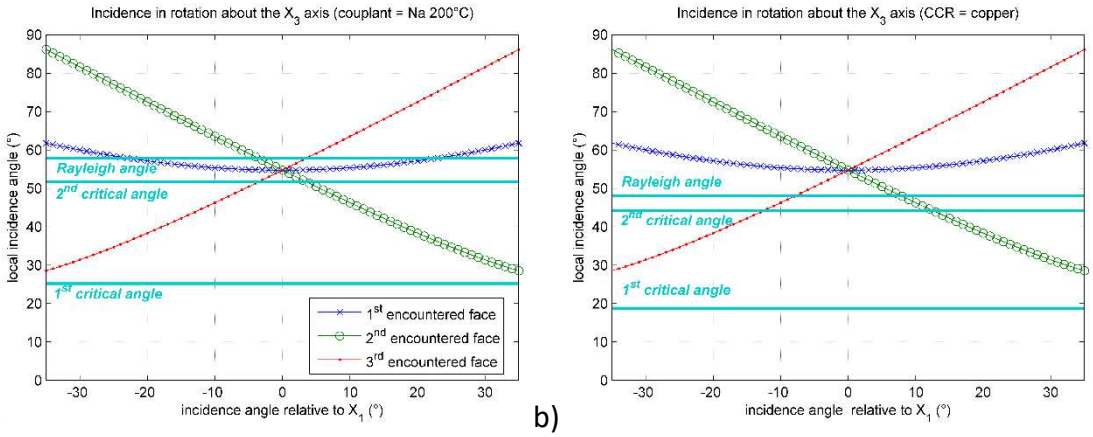

a) b)

Figure 13: Local incidence angles on the faces as a function of initial incidence on CCR (a) for the case of steel in liquid sodium, and(b) for the case of copper in water

The modelled reflection diagram is plotted in Figure 14.b (green curve). This diagram also exhibits a particular behaviour, very different from the case of steel in water. Local minima are found at 0° and 13°, and maxima at 11° and 15°. A CCR made of copper was produced and studied by ultrasound using the same procedure as previously (section 3.1). Experimental results (orange curve) are represented along with modelled results. They are in quite good agreement: the local minimum at 13° and the local maximum at 15° are well recovered. However, the maximum at 11° is experimentally not observed: this incidence angle being in the vicinity of the second critical angle locally on the faces (see Figure 13b), it is outside the limits of validity of CIVA, as mentioned earlier.

These results show that one can always find large angular ranges where high energy is sent back to the transducer. These ranges are reduced compared with those for the

case of steel in water. The knowledge of the media considered for both CCR and surrounding fluid is thus predominant for the overall acoustic reflexion from an immersed CCR.

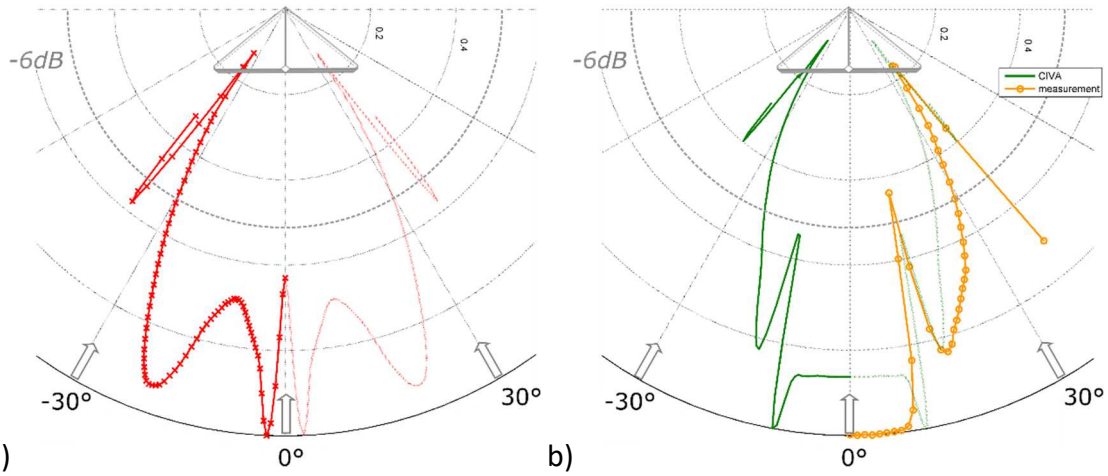

Figure 14: Polar plot of the (normalized) maximum reflected amplitude computed with CIVA (a) for the case of steel in liquid sodium, and (b) for the case of copper in water, with comparison with experimentation

5. Conclusion

The Corner Cube Retroreflector is studied in the framework of ultrasonic telemetry. Its ability to fully reverse an incoming wave in the same direction after three reflections is key to performing telemetry operations (i.e. position measurement) at non-normal incidence (within the angular range of ±30°) on an immersed object. To demonstrate the feasibility of telemetry in various configurations, theoretical developments, modelling and experimentations have been made. It appears possible to locate the steel CCR even behind one and two plates immersed in water, because the amplitude of the back echo is clearly sufficient: SNR equals about 100 for CCR alone, about 50 for

CCR behind a plate, and about 3 for CCR behind two plates. When the CCR is behind screens, the oblique incidence is chosen to maximize the energy transmitted through the screens.

We have also underlined the relevance of considering the acoustic properties of each medium (CCR material and surrounding fluid). They affect the local coefficients of reflection on the CCR faces and thus the global reflection of the target.

Future work will deal with the ability to measure not only the position but also the tilt of a new compact target.

Acknowledgements

This research was supported by the French Alternative Energies and Atomic Energy Commission (CEA) of Cadarache in the framework of the studies for improving In Service Inspection for Generation IV Nuclear Reactors, and within the framework of the MISTRAL joint research laboratory between Aix-Marseille University, CNRS, Centrale Marseille and CEA. The authors also thank Raphaële Raillon and Michel Darmon from CEA-LIST of Saclay Center for their expert help with CIVA calculations.

References

[1] F. Gauche, Generation IV Approach - the Development of Sodium Fast Reactors, Magnetohydrodynamics. 48 (2012) 191–195.

[2] F. Baque, F. Reverdy, J.-M. Augem, J. Sibilo, Development of Tools, Instrumentation and Codes for Improving Periodic Examination and Repair of SFRs, Sci. Technol. Nucl. Install. (2012) 718034. https://doi.org/10.1155/2012/718034.

[3] T. Wang, W. Wang, P. Du, D. Geng, X. Kong, M. Gong, Calculation of the light intensity distribution reflected by a planar corner-cube retroreflector array with the size of centimeter and above, Opt. - Int. J. Light Electron Opt. 124 (2013) 5307–5312. https://doi.org/10.1016/j.ijleo.2013.03.056.

[4] J. Huang, H. Xian, W. Jang, Reflected beam's direction deviation induced by the corner cube retroreflector, in: 2008 Int. Conf. Opt. Instrum. Technol. Optoelectron. Meas. Technol. Appl., 2008: pp. 71601J-71601J–9. https://doi.org/10.1117/12.805917.

[5] Y. Weng, S. Li, H. Zhou, J. Yang, G. Zheng, P. Zhang, Research on far-field diffraction of cube-corner retroreflector in the satellite laser ranging system, in: 5th Int. Symp. Adv.

382 Opt. Manuf. Test. Technol. Opt. Test Meas. Technol. Equip., 2010: pp. 76564R-76564R–8.
383 https://doi.org/10.1117/12.865518.
384 [6] A.L. Whipple, Dynamics of the Earth-Moon system, Adv. Space Res. 13 (1993) 213–219.
385 https://doi.org/10.1016/0273-1177(93)90224-Y.
386 [7] M.C. Garthwaite, S. Nancarrow, A. Hislop, M. Thankappan, J.H. Dawson, S. Lawrie, The
387 Design of Radar Corner Reflectors for the Australian Geophysical Observing System: a
388 single design suitable for InSAR deformation monitoring and SAR calibration at multiple
389 microwave frequency bands., Geosci. Aust. (2015).
390 https://doi.org/10.11636/Record.2015.003.
391 [8] X.-J. Shan, J.-Y. Yin, D.-L. Yu, C.-F. Li, J.-J. Zhao, G.-F. Zhang, Analysis of artificial corner
392 reflector's radar cross section: a physical optics perspective, Arab. J. Geosci. 6 (2013)
393 2755–2765. https://doi.org/10.1007/s12517-012-0582-x.
394 [9] Y. Qin, D. Perissin, L. Lei, The Design and Experiments on Corner Reflectors for Urban
395 Ground Deformation Monitoring in Hong Kong, Int. J. Antennas Propag. 2013 (2013) 1–8.
396 https://doi.org/10.1155/2013/191685.
397 [10] C. Li, J. Yin, J. Zhao, G. Zhang, X. Shan, The selection of artificial corner reflectors based on
398 RCS analysis, Acta Geophys. 60 (2012) 43–58. https://doi.org/10.2478/s11600-011-0060-
399 y.
400 [11] E.F. Knott, J.F. Schaeffer, M.T. Tulley, Radar Cross Section, SciTech Publishing, 2004.
401 [12] D. Devadder, A. Lhemery, New Reflector for Experimental Characterization of Ultrasonic
402 Transducers, J. Phys. 51 (1990) 1295–1298. https://doi.org/10.1051/jphyscol:19902304.
403 [13] C. Locqueteau, Etude des cibles triplanes utilisées en télémétrie ultrasonore, Université
404 d'Aix-Marseille II. Faculté des sciences, 1992.
405 [14] C.G. Stephanis, D.E. Mourmouras, Trihedral rectangular ultrasonic reflector for distance
406 measurements, NDT E Int. 28 (1995) 95–96.

[15] M.M. Narayanan, N. Singh, A. Kumar, C. Babu Rao, T. Jayakumar, An absolute method for determination of misalignment of an immersion ultrasonic transducer, Ultrasonics. 54 (2014) 2081–2089. https://doi.org/10.1016/j.ultras.2014.06.021.

[16] K. Gipson, P.L. Marston, Backscattering enhancements due to retroreflection of ultrasonic leaky Rayleigh waves at corners of solid elastic cubes in water, J. Acoust. Soc. Am. 105 (1999) 700–710. https://doi.org/10.1121/1.426261.

[17] S.S. Dodd, C.M. Loeffler, P.L. Marston, Retroreflective backscattering of sound in water due to Lamb waves on plates with corners: Observations, J. Acoust. Soc. Am. 94 (1993) 1765–1765. https://doi.org/10.1121/1.408070.

[18] P.L. Marston, S.S. Dodd, C.M. Loeffler, Retroflective backscattering of sound in water due to leaky waves on facets, plates, and corner truncations: Approximate theory, J. Acoust. Soc. Am. 94 (1993) 1861–1861. https://doi.org/10.1121/1.407657.

[19] D. Royer, E. Dieulesaint, Ondes Elastiques Dans Les Solides - Tome1 Propagation libre et guidée, Masson, 1996.

[20] T. Pialucha, P. Cawley, An Investigation of the Accuracy of Oblique-Incidence Ultrasonic Reflection Coefficient Measurements, J. Acoust. Soc. Am. 96 (1994) 1651–1660. https://doi.org/10.1121/1.410244.

[21] P. Calmon, S. Mahaut, S. Chatillon, R. Raillon, CIVA: An expertise platform for simulation and processing NDT data, Ultrasonics. 44 (2006) E975–E979. https://doi.org/10.1016/j.ultras.2006.05.218.

[22] M. Darmon, N. Leymarie, S. Chatillon, S. Mahaut, Modelling of scattering of ultrasounds by flaws for NDT, in: A. Leger, M. Deschamps (Eds.), Ultrason. Wave Propag. Non Homog. Media, Springer, Berlin, Heidelberg, 2009: pp. 61–71. https://doi.org/10.1007/978-3-540-89105-5_6.

[23] M. Darmon, S. Chatillon, Main Features of a Complete Ultrasonic Measurement Model: Formal Aspects of Modeling of Both Transducers Radiation and Ultrasonic Flaws Responses, Open J. Acoust. 3 (2013) 43–53. https://doi.org/10.4236/oja.2013.33A008.

[24] M. Darmon, V. Dorval, A. Kamta Djakou, L. Fradkin, S. Chatillon, A system model for ultrasonic NDT based on the Physical Theory of Diffraction (PTD), Ultrasonics. 64 (2016) 115–127. https://doi.org/10.1016/j.ultras.2015.08.006.

[25] L.J. Fradkin, M. Darmon, S. Chatillon, P. Calmon, A semi-numerical model for near-critical angle scattering, J. Acoust. Soc. Am. 139 (2016) 141–150. https://doi.org/10.1121/1.4939494.

[26] A. Imperiale, S. Chatillon, M. Darmon, N. Leymarie, E. Demaldent, UT Simulation Using a Fully Automated 3D Hybrid Model: Application to Planar Backwall Breaking Defects Inspection, in: D.E. Chimenti, L.J. Bond (Eds.), Rev. Prog. Quant. Nondestruct. Eval. Vol 37, 2018: pp. 1–8. https://doi.org/10.1063/1.5031546.

[27] F. Baqué, F. Reverdy, J.-M. Augem, J. Sibilo, Development of Tools, Instrumentation and Codes for Improving Periodic Examination and Repair of SFRs, Sci. Technol. Nucl. Install. (2012) 19. https://doi.org/10.1155/2012/718034.

[28] V. Sobolev, Database of thermophysical properties of liquid metal coolants for GEN-IV, SCK•CEN, Mol, Belgium, 2011. http://hdl.handle.net/10038/7739.

Figures Captions

Figure 1: a) Definition of coordinate system, and normal incidence, referred to as “0°” and b) examples of successive reflections of a ray on the faces with various incidences

Figure 2: Calculation of cylindrical beam reflection as a function of the angle of incidence and the alignment with the inner vertex (the total length of the arrows of one ray travel corresponds to a single time-of-flight)

Figure 3: Reflection coefficient (module and phase) at the water/steel interface as a function of the incidence angle

Figure 4: Local incidence angles on the faces as a function of the initial incidence on CCR

Figure 5: Rotational scan about X3 on CIVA: (a) configuration and (b) polar plot of the maximum received amplitude

Figure 6: Stainless steel CCR and experimental setup

Figure 7: Polar plot of the maximum reflected amplitude: comparison between CIVA simulations and experimentation

Figure 8: Normal incidence Cscan images in amplitude (left) and time-of-flight (right): a) global windowing, b) windowing on CCR inner corner echoes, and c) on CCR edges

Figure 9: Example of Cscan acquisition at oblique incidence (18°): in amplitude (left) and in time-of-flight(right)

Figure 10: Acquisition at normal incidence on the CCR behind a plate (Cscan with narrow time window focused on the first echo from the CCR, between 398.5 and 400 µs)

Figure 11: a) Transmission coefficient (separate contribution of longitudinal and transverse waves) through a steel plate immersed in water. b) Angle of propagation in the plate, as a function of the incidence angle

Figure 12: Acquisition at oblique incidence (18°) on the CCR behind a plate

Figure 13: Local incidence angles on the faces as a function of initial incidence on CCR (a) for the case of steel in liquid sodium, and(b) for the case of copper in water

Figure 14: Polar plot of the maximum reflected amplitude computed with CIVA (a) for the case of steel in liquid sodium, and (b) for the case of copper in water, with comparison with experimentation

Tables Captions

Table 1: Signal-to-noise ratio of the back echoes from the CCR according to configuration